

Analysis of vortex induced vibration frequency of super tall building based on wind tunnel tests of MDOF aero-elastic model

Lei Wang^{1,2}, Shuguo Liang^{*1}, Jie Song¹ and Shuliang Wang¹

¹School of Civil & Building Engineering, Wuhan University, Wuhan 430072, China

²School of Civil Engineering, Henan Polytechnic University, Jiaozuo 454000, China

(Received January 30, 2015, Revised July 15, 2014, Accepted September 1, 2015)

Abstract. To study the vibration frequency of super high-rise buildings in the process of vortex induced vibration (VIV), wind tunnel tests of multi-degree-of-freedom (MDOF) aero-elastic models were carried out to measure the vibration frequency of the system directly. The effects of structural damping, wind field category, mass density, reduced wind velocity (V_r), as well as VIV displacement on the VIV frequency were investigated systematically. It was found that the frequency drift phenomenon cannot be ignored when the building is very high and flexible. When V_r is less than 8, the drift magnitude of the frequency is typically positive. When V_r is close to the critical wind velocity of resonance, the frequency drift magnitude becomes negative and reaches a minimum at the critical wind velocity. When V_r is larger than 12, the frequency drift magnitude almost maintains a stable value that is slightly smaller than the fundamental frequency of the aero-elastic model. Furthermore, the vibration frequency does not lock in the vortex shedding frequency completely, and it can even be significantly modified by the vortex shedding frequency when the reduced wind velocity is close to 10.5.

Keywords: super high-rise building; vortex-induced vibration; multi-degree-of-freedom model; aerodynamic stiffness; frequency drift phenomenon

1. Introduction

Flexible high-rise buildings may be exposed to the danger of vortex-induced vibration, when the vortex shedding frequency is close to the natural frequency of the building, i.e., the lock-in phenomenon may take place. It is usually assumed that the aerodynamic stiffness and aerodynamic mass, which may change the frequency of the associated vibration system, are insignificant in the VIV process (Vikestad *et al.* 2000, LI *et al.* 2011, Kwok and Melbourne 1981, Larsen 1995).

In fact, when a tall building is in the state of the vortex induced resonance or close to the state, the aerodynamic stiffness is likely to be significant, especially when the flexibility of the building exceeds a certain value. Some researchers have investigated the effects of the aerodynamic stiffness in VIV: as a linear term, aerodynamic stiffness was taken into account in several semi-empirical models based on Van der Pol oscillator to assess VIV responses (Simiu and Scanlan 1986, Basu and Vickery 2011, Goswami *et al.* 1981, Larsen 1995, Chen *et al.* 1997).

*Corresponding author, Professor, E-mail: liangsgwhu@sohu.com.cn

Stekley and Vickery (1990, 1993) have studied the aerodynamic stiffness and mass by forced vibration tests, through which the frequency drift magnitude was estimated. In addition, a V-shape relationship between the aerodynamic stiffness and reduced wind velocity was found by Stekley and Vickery. Tamura and Sukanuma (1996) also studied the frequency drift phenomenon on the basis of full scale measurements on many tall buildings, for cases where the approaching wind is not perpendicular to one of the vertical faces of the building.

As mentioned above, although the effects from aerodynamic stiffness and mass have been noted by a few researchers, the investigation is seldom conducted based on the multi-degree of freedom (MDOF) system. In fact, wind tunnel tests of the MDOF model are more reliable for the VIV, because the VIV frequency can be determined directly and precisely as well as different test conditions can be easily arranged by an accurate measurement and simulation. Therefore, the MDOF model is adopted in this study to investigate the frequency drift phenomenon in the VIV process.

2. Wind tunnel test

The wind tunnel test was conducted in the boundary layer wind tunnel of Wuhan University, China. The wind tunnel is a straight flow, low-velocity wind tunnel. The cross-section of the wind tunnel is 3.2 m wide \times 2.1 m high. Two terrain categories (i.e., terrain category B and D in China's Code 2012) were simulated using a set of spires and roughness elements in front of the building models. The mean velocity profiles and turbulence intensity in the wind tunnel are illustrated in Fig. 1 for the two categories respectively.

Three types of MDOF aero-elastic models were installed in the wind tunnel respectively. The models were square prisms with aspect ratios of 10, 13, and 16, respectively. Each model was fabricated as a six-lumped-mass system to simulate super-high-rise buildings of 600 m, 780 m, and 900 m high respectively. The skeleton of the MDOF models consisted of aluminum columns and rigid plates. Striking a balance between the blockage ratio requirements and easy operation, a length scale of 1: 600 was adopted. Three models shared the same similarity and the similarity ratios are shown in Table 1.

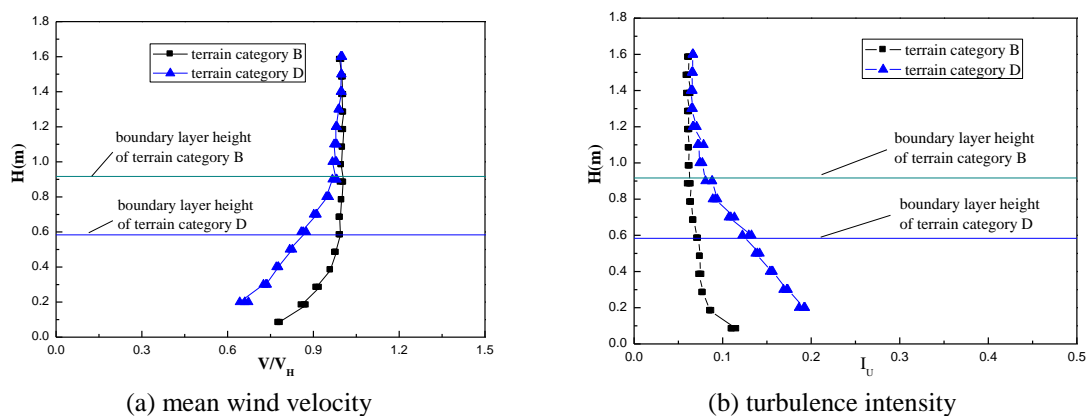


Fig. 1 Mean wind velocity and turbulence intensity profiles

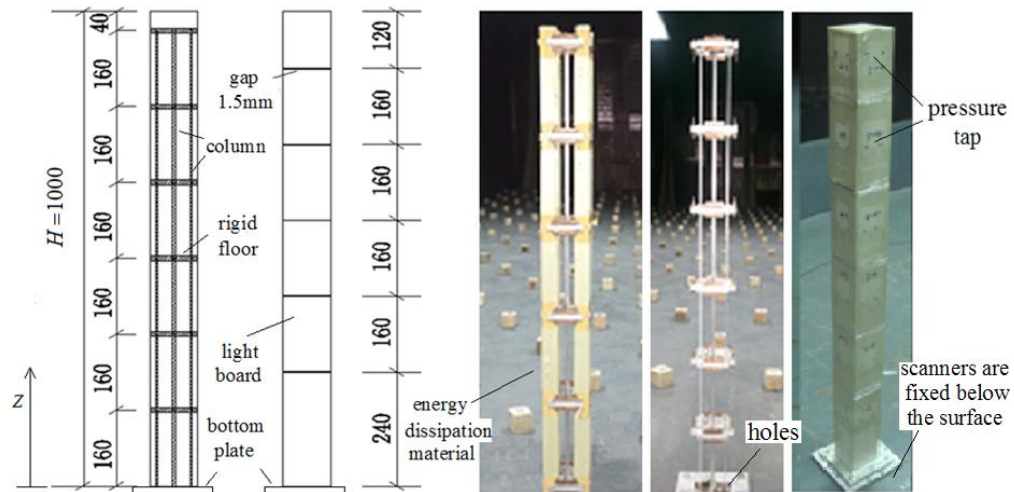


Fig. 2 Outline of the model (aspect ratio=10) (unit: mm)

Fig. 2 shows the model with an aspect ratio of 10. As can be seen, each floor was drilled with holes and connected by five fitted aluminum columns, including one thick column in the center and four flexible columns in the four edges, to adjust the sway modes and stiffness parameters. The trim copper billet was fixed on each floor to adjust the required mass and mass moment of inertia. The additional damping was provided by energy-dissipation material attached to the surface of each floor. The dynamic properties of each MDOF model are presented in Table 2. In the table, the natural frequency is the fundamental frequency, i.e., the vibration frequency of the first mode.

To measure the wind pressure on the surfaces of each model, 72 pressure transducers were installed over the surfaces of the model, and their instantaneous pressures were synchronously scanned by a scanning valve system. Meanwhile, the displacement response at the top of the model was measured by a laser displacement sensor. It should be mentioned that to eliminate the influence of the pressure scanners and 72 plastic tubes on the model's dynamic properties, the scanners were fixed below the surface of the wind tunnel floor through the pre-set holes as shown in Fig. 2. In addition, the plastic tubes were tied to the thick column.

Table 1 Similarity parameters

| Property | Modeling parameters | Scale |
|-----------|---------------------|-------|
| Length | l_m / l_p | 1/600 |
| Frequency | n_m / n_p | 100 |
| Velocity | V_m / V_p | 1/6 |
| Density | ρ_m / ρ_p | 1 |

Note: Subscript m and p denote model and prototype building, respectively

Table 2 Dynamic parameters of the MDOF aero-elastic models

| Test condition | Geometric size | 1 st natural frequency | Equivalent mass | Damping ratio | Scruton number |
|----------------|----------------|-----------------------------------|-----------------|---------------|----------------|
| 1 | 1.0×0.1 m | 9.89 Hz | 2.27 kg/m | 0.7% | 2.50 |
| 2 | 1.0×0.1 m | 10.18 Hz | 1.85 kg/m | 1.1% | 3.25 |
| 3 | 1.0×0.1 m | 9.64 Hz | 2.27 kg/m | 1.8% | 6.34 |
| 4 | 1.0×0.1 m | 9.27 Hz | 2.27 kg/m | 3.6% | 13.05 |
| 5 | 1.0×0.1 m | 9.40 Hz | 2.50 kg/m | 3.6% | 14.40 |
| 6 | 1.0×0.1 m | 8.19 Hz | 3.00 kg/m | 4.5% | 20.64 |
| 7 | 1.3×0.1 m | 10.83 Hz | 1.31 kg/m | 1.02% | 2.14 |
| 8 | 1.3×0.1 m | 9.02 Hz | 1.31 kg/m | 2.89% | 6.05 |
| 9 | 1.3×0.1 m | 10.6 Hz | 1.31 kg/m | 1.43% | 2.99 |
| 10 | 1.3×0.1 m | 8.70 Hz | 2.17 kg/m | 3.72% | 12.91 |
| 11 | 1.3×0.1 m | 7.17 Hz | 2.38 kg/m | 4.50% | 17.06 |
| 12 | 1.6×0.1 m | 7.14 Hz | 1.25kg/m | 0.82% | 1.64 |
| 13 | 1.6×0.1 m | 5.98 Hz | 1.81 kg/m | 0.82% | 2.38 |
| 14 | 1.6×0.1 m | 7.02 Hz | 1.25 kg/m | 1.33% | 2.60 |
| 15 | 1.6×0.1 m | 5.19 Hz | 2.38 kg/m | 1.11% | 4.25 |
| 16 | 1.6×0.1 m | 5.68 Hz | 2.38 kg/m | 1.71% | 6.31 |
| 17 | 1.6×0.1 m | 5.07 Hz | 2.38kg/m | 2.30% | 8.75 |

Note: Here the item equivalent mass(M) and Scruton number(Sc) can be expressed by Eqs. (1) and (2), respectively

$$M = \frac{\int_0^L m(z)\phi^2(z) dz}{\int_0^H \phi^2(z) dz} \quad (1)$$

$$Sc = \frac{2M\xi_s}{\rho_a D^2} \quad (2)$$

where $m(z)$ and $\phi(z)$ are the mass per unit length and the mode shape of the model, respectively; H is the height of the models; ξ_s , ρ_a , and D are the structural damping ratio, air density, and width of the model, respectively.

3. VIV response of MDOF model

In this section, the VIV response of the MDOF model is investigated, in terms of the standard deviation(STD) of the crosswind displacement response (σ_y), as shown in Fig. 3. It has been well acknowledged that the resonance may occur when the vortex shedding frequency is close to the structural frequency (Bearman 1984, Larsen 1995, Melbourne 1997). In other words, resonance

may occur when V_r (defined in Eq. (3)) is close to critical reduced velocity of resonance, which is about 10.5 for square prisms in uniform flow.

$$V_r = \frac{V}{n_1 D} \tag{3}$$

where V , n_1 , and D denote mean wind speed, system vibration frequency of the 1st mode, and windward side width of the MDOF model, respectively.

Resonance has been found to be sensitive to the aspect ratio, mass density and inherent damping of the structure. As can be seen from Fig. 3, the results from the wind tunnel measurement are consistent with the reported results (Bearman 1984, Larsen 1995, Melbourne 1997). Actually, Fig. 3 shows that the displacement responses in both of the two types of flow present a remarkable peak. Furthermore, the peak in uniform smooth flow is much sharper than that in turbulent flow. The smaller the Scruton number S_c is, the greater the VIV responses will be.

4. Frequency drift phenomenon

The non-dimensional drift of the system frequency is defined as

$$\delta_n = (n_1 - n_0) / n_0 = n_1 / n_0 - 1 \tag{4}$$

where n_0 denotes the natural frequency of the 1st mode of the MDOF model.

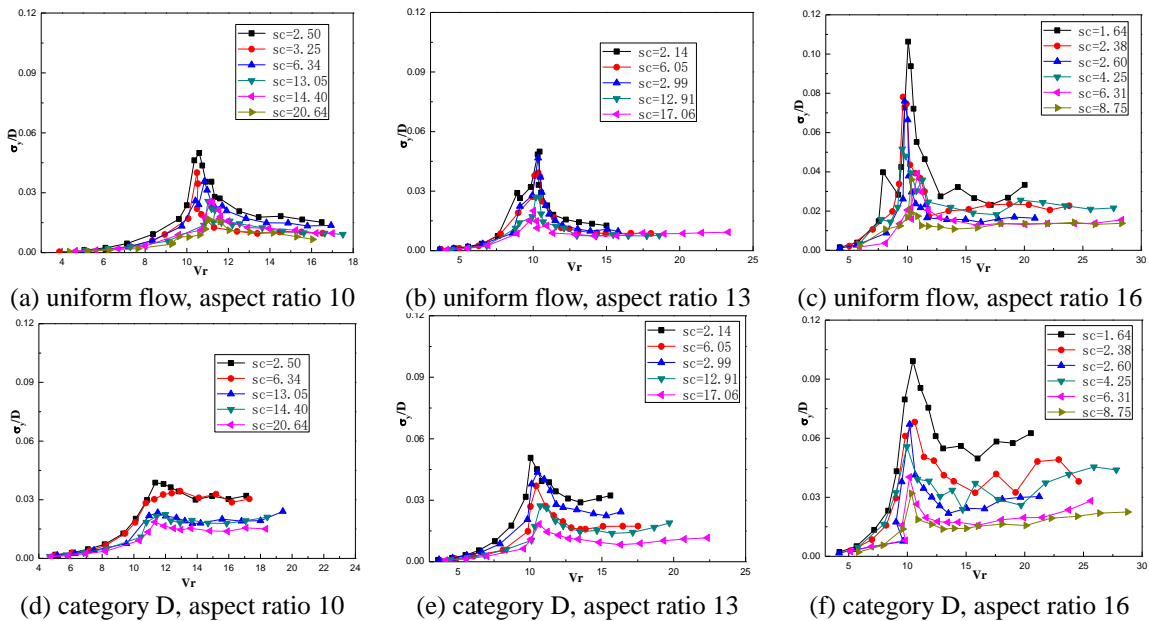


Fig. 3 Cross-wind displacement response of each MDOF model

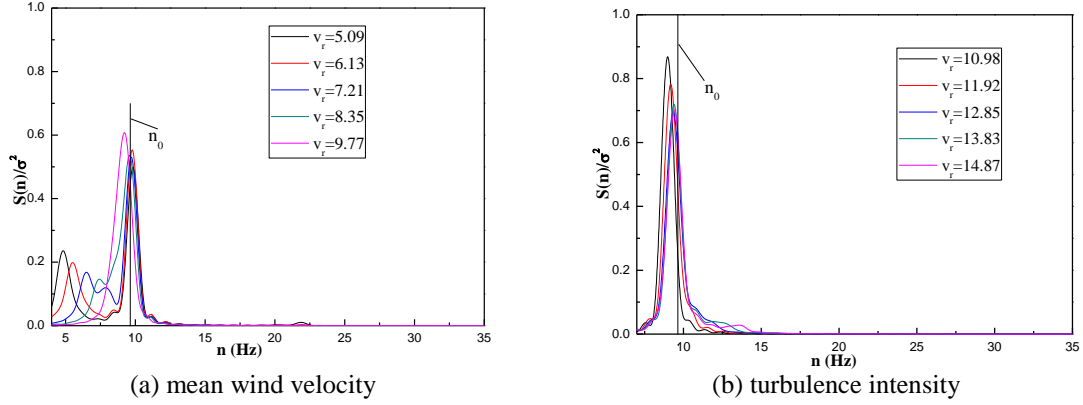


Fig. 4 Response spectra of MDOF models at different reduced wind velocities (test condition 3 in uniform flow)

Fig. 4 shows the response spectra of the MDOF model with different V_r . As can be seen, the vibration of the first mode of the MDOF model is dominant, whereas the vibration of the second mode whose frequency is about 35 Hz is marginal and can be ignored. According to Fig. 4, the vibration frequency can be identified and the corresponding results of vibration frequency are shown in Fig. 5 as a function of V_r . As can be seen from Fig. 5, when V_r is less than 8, the drift magnitude of the frequency is normally positive. However, when V_r is close to critical wind velocity of resonance (10.5), drift magnitude of frequency turns to be negative and reaches a minimum at the critical wind velocity. When V_r is larger than 12, the drift magnitude becomes relatively stable, approximating a value which is slightly smaller than the fundamental frequency of MDOF model.

The above findings are compared with those reported by Vickery *et al.* (1993) for the aerodynamic stiffness of forced vibration tests, as shown in Fig.6. In Vickery's study (i.e., Fig. 6(a)), α is an aerodynamic stiffness parameter, the relationship between α and δ_n can be deduced as follows:

Firstly, α is derived from the definition of Vickery *et al.* (1993), which can be expressed as

$$\alpha = \frac{K_a \times \rho_s}{2K_s \times \rho_a} \quad (5)$$

where K_a and K_s denote aerodynamic stiffness and building stiffness, respectively; ρ_a and ρ_s denote the air density and building density, respectively.

The fundamental frequency of the test model can be expressed as

$$n_0 = \frac{1}{2\pi} \sqrt{K_1^* / M_1^*} \quad (6)$$

where K_1^* and M_1^* denote generalized stiffness and generalized mass of the first mode, respectively. For Vickery's forced vibration test, the item K_s in Eq. (5) have the same meaning as K_1^* ,

accordingly, K_a is also a generalized parameter, which can be directly added to generalized stiffness K_1^* .

So the system vibration frequency of the 1st mode n_1 can be expressed as

$$n_1 = \frac{1}{2\pi} \sqrt{(K_1^* + K_a) / M_1^*} \tag{7}$$

Then the relationship between α and δ_n can be deduced as

$$\delta_n = \frac{n_1}{n_0} - 1 = \frac{2\pi \sqrt{(K_1^* + K_a) / M_1^*}}{2\pi \sqrt{K_1^* / M_1^*}} - 1 = \sqrt{1 + K_a / K_1^*} - 1 = \sqrt{1 + (2\rho_a / \rho_s) \times \alpha} - 1 \tag{8}$$

Based on above deduced results and the data of α in Fig. 6(a), the corresponding δ_n can be easily calculated (as shown in Fig. 6(b)). It can be seen that the two sets of the results show similar variations, although the drift magnitude of this study is slightly larger than Vickery's.

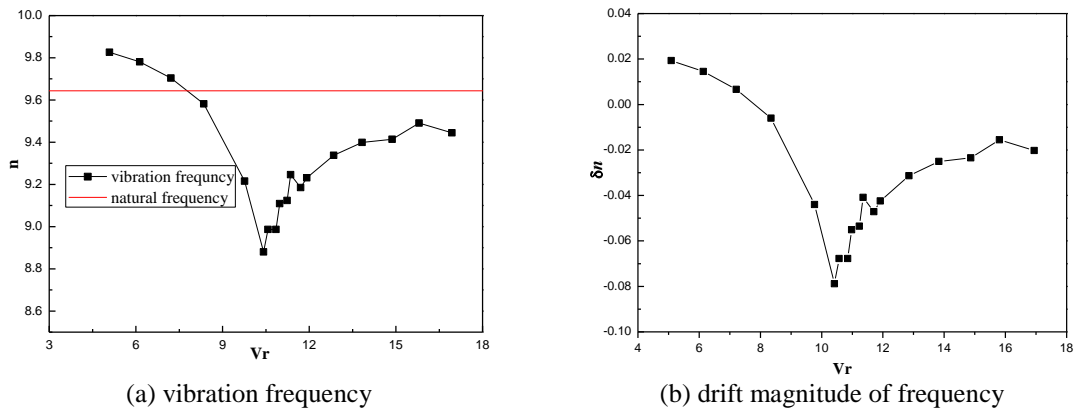


Fig. 5 Deviation of frequencies varying with Vr

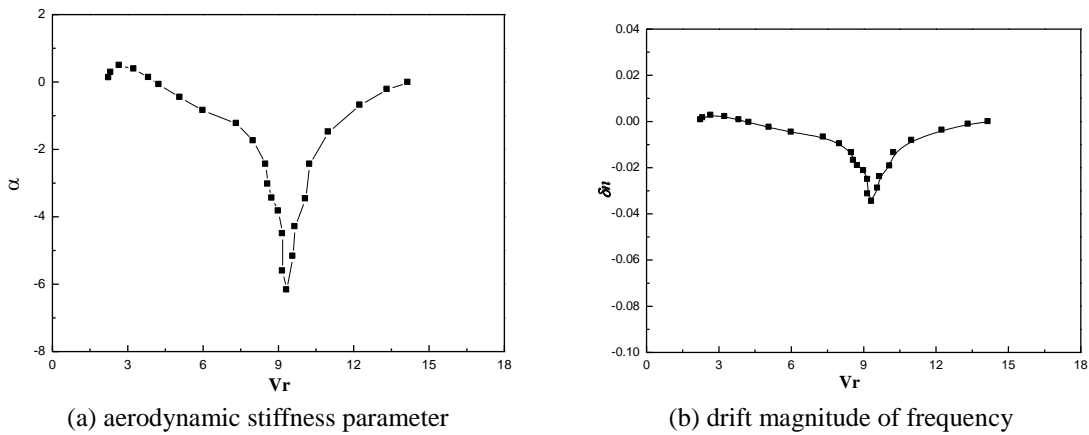


Fig. 6 Aerodynamic stiffness and drift magnitude of frequency according to Vickery *et al.* (1993)

5. Effects of model parameters on drift magnitude of VIV frequency

5.1 Structural mass

Fig.7 shows δ_n of the MDOF model with different values of structural mass m . As can be seen, the absolute value of δ_n for the model with a small mass density is greater than that for the model with a relatively large mass density. This phenomenon is more obvious at the critical reduced wind speed. In fact, the VIV response of a model with a small m is greater than that with a large m . Therefore, the aerodynamic stiffness of a light model is also greater than that of a heavy model. Accordingly, the change of the vibration frequency of the light model is more significant than that of the heavy model.

5.2 Wind field category

Fig. 8 shows values of δ_n in wind fields with different terrain category. As can be seen, the curve of δ_n in uniform smooth flow is more close to a V-shape than that in the turbulence flow. More specifically, when V_r is less than 8 or larger than 12, the absolute value of δ_n is more significant in turbulence flow; when V_r is close to 10.5, the absolute value of δ_n is more remarkable in uniform smooth flow.

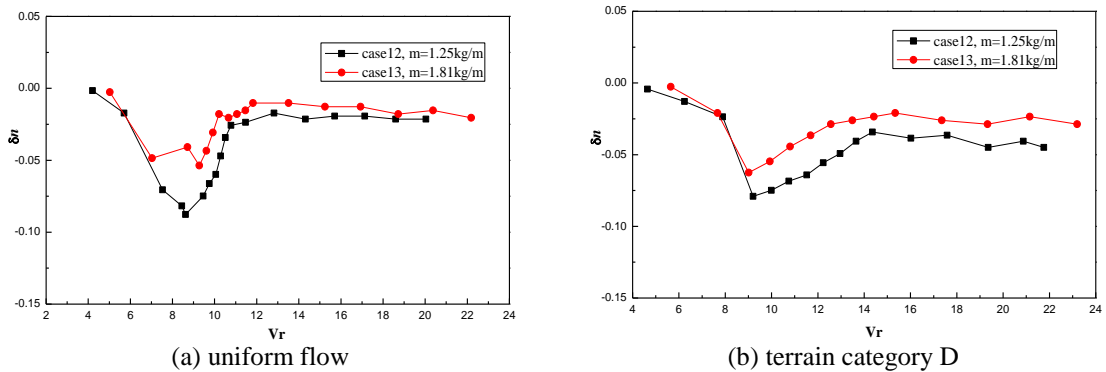


Fig. 7 Drift magnitude of vibration frequency as a function of V_r for two values of m

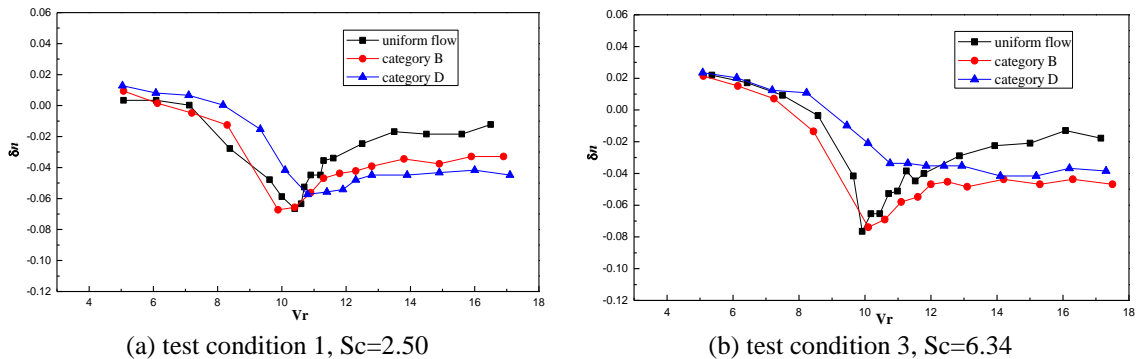


Fig. 8 Drift magnitude of vibration frequency in wind field with different roughness

5.3 Structural damping ratio

The values of δ_n for different structural damping ratios are shown in Fig. 9. As can be seen, below the resonance wind velocity, the value of δ_n for the large damping ratio is slightly larger than that for the small damping ratio. By contrast, when V_r is very close to the resonance wind velocity, the absolute value of δ_n for the large damping ratio is far greater than that for the small damping ratio. When V_r is larger than 13, however, the difference between the two curves is relatively insignificant.

5.4 Aspect ratio

The effects of aspect ratio on the drift magnitude are investigated in this section. The drift magnitudes for two scenarios (i.e., $H/D = 10$ and 16) are presented in Fig. 10. As can be seen, when V_r is smaller than 7 or larger than 11, the absolute value of δ_n for the large aspect ratio (i.e., $H/D = 16$) is relatively small. However, when V_r is close to the resonance wind velocity, the difference between the minimum values of δ_n for the two different aspect ratios is slight. Therefore, it can be concluded that the V-shape of the model with a large aspect ratio is sharper than that of a small aspect ratio model.

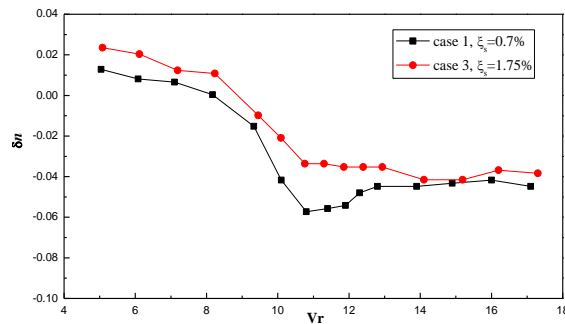


Fig. 9 Drift magnitude of frequency with different structural damping ratios (terrain category D)

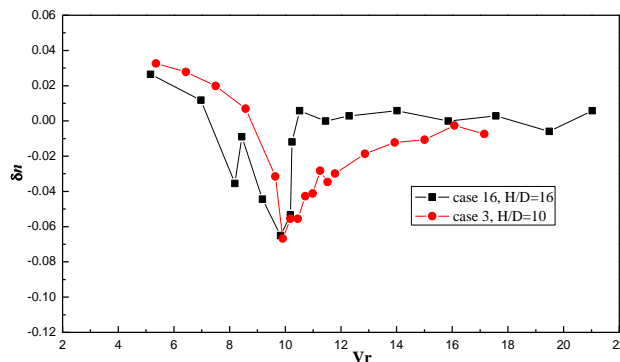


Fig. 10 Drift magnitude of VIV frequency with different structure damping (uniform flow)

5.5 The relationship between δ_n and STD of displacement response

Figs. 11 and 12 show the relationship between the vibration frequency and STD of the displacement response. As can be seen from Fig. 11, the curve of STD of the displacement response against V_r shows an inverted V-shape, whereas the curve of vibration frequency is a normal V-shape. It seems that the two curves are largely symmetrical. As can be seen from Fig. 12, the vibration frequency of the model generally decreases with increasing STD of the displacement response. The decrease is more significant in turbulent flow. For instance, Fig. 12(b) shows that the vibration frequency almost monotonously decreases with increasing STD of the displacement response. This finding is very similar to that reported by Tamura (1996), as shown in Fig. 13, which partly validates the accuracy of measured data. It should be mentioned that there are a few discontinuous points in Fig. 12(a). It is interesting that the values of V_r associated with these discontinuous points are close to the critical reduced wind velocity.

According to the VIV mechanism, the VIV displacement response is negatively correlated to aerodynamic stiffness and δ_n . As a result, significant VIV displacement responses will cause reduction of the system stiffness, because of negative aerodynamic stiffness. The reduction in system stiffness in turn tends to increase the VIV displacement responses, which is so-called self-excited phenomenon. Furthermore, alterations of system stiffness will change the vibration frequency of the system. Meanwhile, the alterations of vibration frequency will affect the vortex shedding frequency. Consequently, the vortex shedding frequency and vibration frequency of the system finally converge to a stable value, or fluctuate around the value slightly.

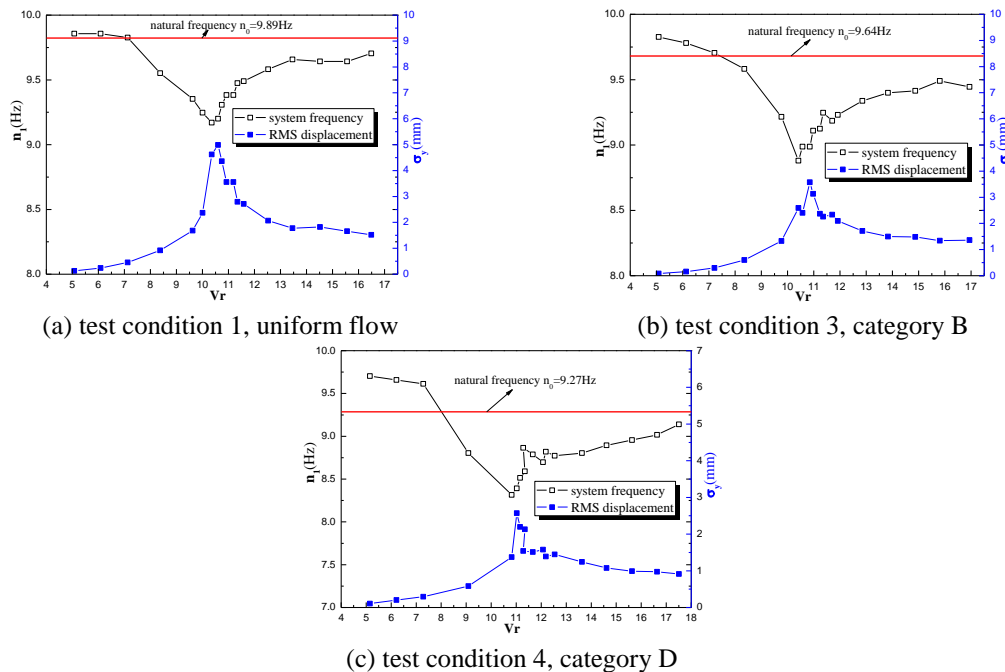


Fig. 11 Vibration frequency and STD displacement

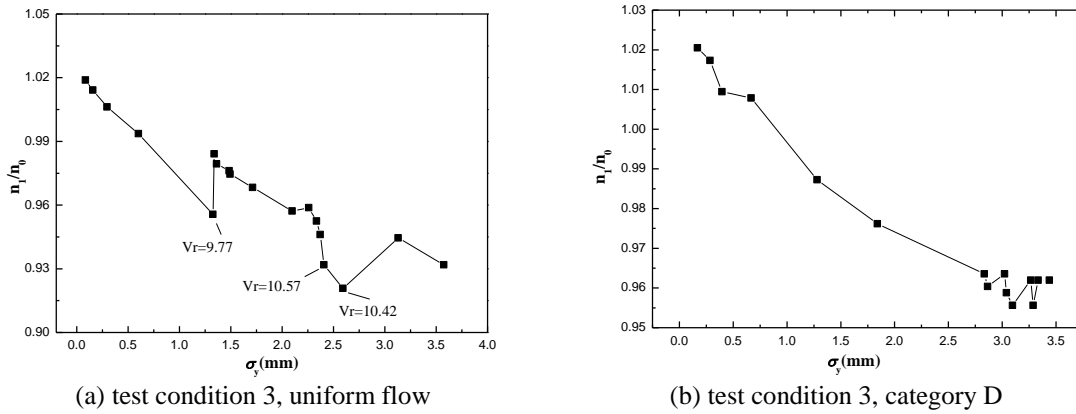


Fig. 12 The parameter n_1/n_0 varying with STD displacement

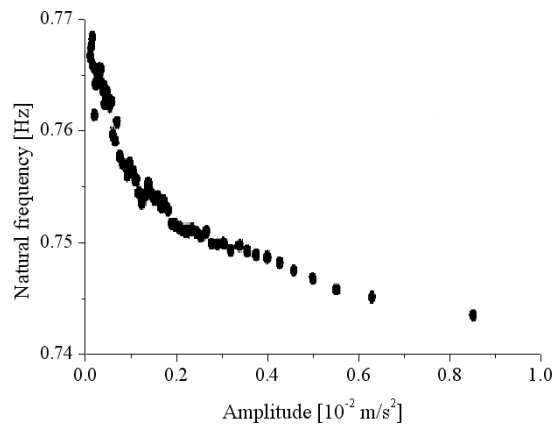


Fig. 13 Full-scale measured frequency of a tower by Tamura

It should be mentioned that in fact, when V_r is relatively small (e.g., $V_r=5.09, 6.13, 7.21, 8.35$), the VIV response spectrum shows two peaks, as shown in Fig. 4. These two peaks indicate the vortex shedding frequency and the vibration frequency of the system, respectively. However, when V_r is close to the critical velocity (e.g., $V_r=9.77$), the two peaks converge to one peak.

6. Relationship between VIV frequency and vortex shedding frequency

Fig. 14 shows the relationship between the vibration frequency of the system and the vortex shedding frequency (test condition 7), where the vortex shedding frequency was identified from the wind pressure spectra. As can be seen from Fig. 14, when the reduced wind velocity is less than 10, the vortex shedding frequency is far smaller than the vibration frequency of the system. This means lock-in phenomenon does not occur within this range. By contrast, when the reduced velocity is within 10.3~11, the vortex shedding frequency is just slightly smaller than the vibration

frequency of the system. It is interesting to note that when reduced wind velocity is larger than 11, the vortex shedding frequency shows a significant increase with V_r and becomes much larger than the vibration frequency of the system. In summary, the vibration frequency does not completely coincide with the vortex shedding frequency. The vibration frequency of the system may be affected by the vortex shedding frequency, especially when reduced wind velocity is around 10.5. Although the vortex shedding frequency is very close to the vibration frequency of the system, these two frequencies are not perfectly equal. Therefore, the resonance phenomenon in this study is not an ideal lock-in phenomenon as shown in Fig. 15.

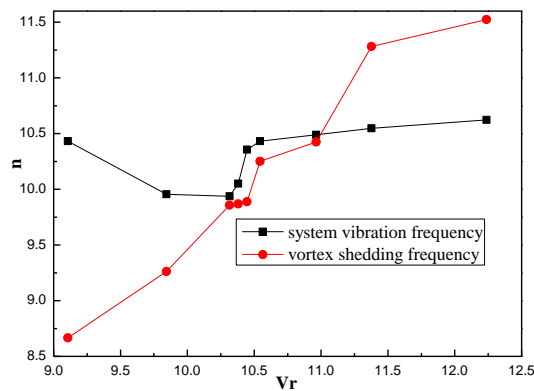


Fig. 14 Frequencies of VIV and vortex shedding (test condition 7)

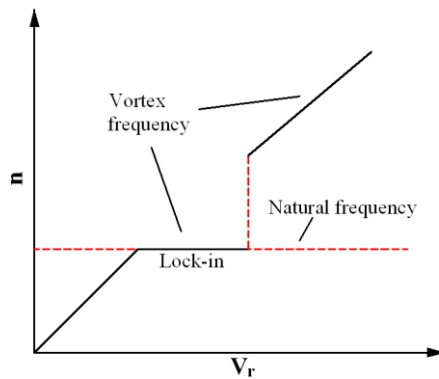


Fig. 15 Frequencies of ideal lock-in phenomenon

7. Conclusions

The main findings from this investigation are summarized as follows:

(1) For high flexible tall buildings, the aerodynamic stiffness cannot be ignored. Due to the aerodynamic stiffness, the VIV frequency can deviate from the structural natural frequency by as

high as 10%. The drift magnitude of vibration frequency is a V-shape curve, and the minimum frequency is located at the critical wind speed of vortex shedding.

(2) The VIV displacement response is negatively correlated to the aerodynamic stiffness and vibration frequency. In view of the negative aerodynamic stiffness, a significant VIV displacement response will result in reduction in system stiffness. In turn, the reduction in system stiffness tends to increase VIV displacement response, which is so-called self-excited phenomenon.

(3) The resonance induced by vortex shedding is not an ideal lock-in phenomenon, and the vibration frequency does not lock in the vortex shedding frequency completely. The vibration frequency of the system can also be affected by the vortex shedding frequency, especially when the reduced wind velocity is close to 10.5. In fact, the vortex shedding frequency usually approaches to the natural frequency of the system, but these two frequencies are not perfect equal, albeit very close.

(4) Due to the self-limiting and nonlinearity of VIV mechanism and the relationship between the STD of VIV displacement response and the aerodynamic stiffness, the aerodynamic stiffness and drift magnitude of system frequency are highly sensitive to the aspect ratio, mass density, inherent damping of structure, as well as the roughness of wind field. Therefore, a novel model which can consider the nonlinear aerodynamic stiffness is necessary to assess vortex-induced resonance responses of high-rise flexible building accurately.

Acknowledgments

The investigation presented in this paper was supported by the China National Natural Science Foundation under project No. 51178359, which is gratefully acknowledged.

References

- Basu, R.I. and Vickery, B.J. (1983), "Across-wind vibrations of structures of circular cross-section—part 2: development of a mathematical model for full-scale application", *J. Wind Eng. Ind. Aerod.*, **12**(1), 1275-1297
- Bearman, P.W. (1984), "Vortex shedding from oscillating bluff bodies", *Annu. Rev. Fluid Mech.*, **16**, 195-222.
- Chen, R., Cheng, C. and Lu P. (1997). "Wind-structure interaction of a high-rise building in boundary layer flows", *J. Chinese Inst. Civil Hydraulic Eng.*, **9**(2), 271-279.
- GB50009-2012 (2012), *Load Code for the Design of Building Structures*, China Architecture and Building Press, Beijing, China.
- Goswami, I., Scanlan, R.H. and Jones, N.P. (1993), "Vortex-induced vibration of circular cylinders—part 2: new model", *J. Eng. Mech. - ASCE*, **119**(11), 2288-2302.
- Kwok, K.C.S. and Melbourne, W.H. (1981), "Wind-induced lock-in excitation of tall structures", *J. Struct. Div. - ASCE*, **107**(1), 58-72.
- Larsen, A. (1995), "A generalized model for assessment of vortex-induced vibration for flexible structures", *J. Wind Eng. Ind. Aerod.*, **57**(2-3), 281-294.
- Li, Y., Wang, L. and Shen, Z. (2011), "Added-mass estimation of flat membranes vibrating in still air", *J. Wind Eng. Ind. Aerod.*, **99**(8), 815-824.
- Melbourne, W. H. (1997), "Predicting the cross-wind response of masts and structural members", *J. Wind Eng. Ind. Aerod.*, **69-71**, 91-103.
- Simiu, E. and Scanlan, R.H. (1986), *Wind Effects on Structures*, Wiley, New York.

- Stekley, A. and Vickery B.J. (1990), "On the measurement of motion induced force on models in turbulent shear flow", *J. Wind Eng. Ind. Aerod.*, **36**, 339-350.
- Tamura, Y. and Sugauma, S. (1996), "Evaluation of amplitude-dependent damping and natural frequency of buildings during strong winds", *J. Wind Eng. Ind. Aerod.*, **59**(2-3), 115-130
- Vickery, B.J., Stekley, A. and Isyumov, N. (1993), "Aerodynamic damping and vortex excitation on an oscillating prism in turbulent shear flow", *J. Wind Eng. Ind. Aerod.*, **49**(1-3), 121-140.
- Vikestad, K., Vandiver, J.K. and Larsen, C.M. (2000), "Added mass and oscillation frequency for a circular cylinder subjected to vortex-induced vibrations and external disturbance", *J. Fluid. Struct.*, **14**(7), 1071-1088.